GIADA - Grain Impact Analyzer and Dust Accumulator - onboard Rosetta spacecraft: extended calibrations.

V. Della Corte,[a,1,*], R. Sordini[a,1], M. Accolla[b,2], M. Ferrari[a,1], S. Ivanovski[a,1], A. Rotundi[c,a,3,1], F.J.M. Rietmeijer[d,4], M. Fulle[e,5], E. Mazzotta-Epifani[f,6], P. Palumbo[c,a,3,1], L. Colangeli[h,7], J. J. Lopez-Moreno[g,8], J. Rodriguez[g,8], R. Morales[g,8], M. Cosi[i,9]

[a] *Via del Fosso del Cavaliere 100, Roma*
[b] *Via S. Sofia 78, Catania*
[c] *CDN Isola C4, Napoli*
[d] *Albuquerque, NM 87131-0001, USA*
[e] *Via Tiepolo 11, 34143 Trieste, Italy*
[f] *Via Frascati 33, 00078, Monte Porzio Catone (RM)*
[g] *P.O. Box 3008, 18080 Granada, Spain*
[h] *Keplerlaan 1, 2201 AZ Noordwijk, Netherlands*
[i] *Via A. Einstein, 35, 50013 - Campi Bisenzio (Firenze), Italy*

Abstract

Despite a long tradition of dust instruments flown on-board space mission, the largest number of these can be considered unique as they used different detection techniques. GIADA (Grain Impact Analyzer and Dust Accumulator), is one of the dust instruments on-board the Rosetta spacecraft and is devoted to measure the dust dynamical parameters in the coma of comet 67P/Churyumov-Gerasimenko. It couples two different techniques to mea-

*Corresponding author
URL: vincenzo.dellacorte@iaps.inaf.it (V. Della Corte,)
[1]INAF- Instituto Astrofisica e Planetologia Spaziali
[2]INAF- Osservatorio Astrofisico di Catania
[3]Universitá di Napoli "Parthenope"
[4]Dept. of Earth and Planetary Science MSC 03 2040, University of New Mexico
[5]INAF-Osservatorio Astronomico di Trieste
[6]INAF-Osservatorio Astronomico di Roma
[7]ESA, European Space Research and Technology Centre (ESTEC)
[8]Instituto de Astrofisica de Andalucia, Consejo Superior de Investigaciones Cientificas (CSIC)
[9]Selex-ES

sure the mass and speed of individual dust particles. We report here the results of an extended calibration activity carried-out, during the hibernation phase of the Rosetta mission, on the GIADA Proto Flight Model (PFM) operative in a clean room in our laboratory. The main aims of an additional calibration campaign are:

- to verify the algorithms and procedures for data calibration developed before Rosetta launch;
- to improve the comprehension of GIADA response after the increased knowledge on cometary dust, e.g. the composition of dust particles after Stardust mission.

These calibration improvements implied a final step, which consisted in defining transfer functions to correlate the new calibration curves obtained for the GIADA PFM to those to be used for GIADA onboard the Rosetta spacecraft. The extended calibration activity allowed us to analyse GIADA data acquired in the 67P/C-G coma permitting to infer additional information on cometary dust particles, e.g. density and tensile strength.

Keywords:
Rosetta Esa Mission; GIADA; Dust dynamical properties;
Calibration;Comet;Coma dust environment;

---

1. Introduction

Cosmic dust can be studied in laboratory (e.g. (1; 2; 3)) after returning it to Earth using a variety of collection methods: dedicated collectors flown by stratospheric aircrafts (4); balloon-borne instruments (5); spacecraft flying through cometary comae (6) or collecting dust on asteroid surface (7). Dust can also be studied "in-situ" in cometary dust environments (8; 9; 10; 11; 12) and in the interplanetary medium by space instruments exploiting physical processes able to reveal the presence of dust particles. In-situ dust detectors are generally devised to measure parameters associated with high-velocity dust impacts to then derive the particle physical properties, with the support of laboratory calibration activity, e.g. impacting accelerated particles with known physical-chemical properties onto a laboratory replica of the dust detector. Space dust instruments have measured for instance the impact light flash, acoustic signal and impact ionization (13; 14). They were mounted

on-board various space probes: the HEOS-2 (15), Helios (16), Pioneer 10, Pioneer 11 (17), Giotto (12), Ulysses (14), Galileo, Stardust (13; 14; 18) and LADEE (19). Dust detectors were also operating onboard Earth-orbiting satellites as LDEF, EURECA, and Gorid satellites (20). Presently dust instruments are flying on the Cassini, New Horizon (21) and Rosetta spacecrafts. Three dust instruments flying onboard the Rosetta space probe of the European Space Agency (ESA) are designed to characterise in-situ the dust particles emitted by 67P/Churyumov-Gerasimenko (hereafter 67P/C-G) nucleus. Among them GIADA (Grain Impact Analyzer and Dust Accumulator) (Fig. 1), is devoted to analyse the comet particles physical dynamical parameters measuring the speed and the momentum of each particle entering the instrument, and the fluence of the fine dust particles, with size ≤ 5 microns (22; 23).

2. GIADA Instrument

GIADA consists of three different detection subsystems assembled in a single instrument with specific relative geometrical positions that allows combined measurements. The three detections sub-systems are: (1) the Grain Detection System (GDS), devoted to detect individual particle entering GIADA without affecting its dynamic properties and to constraint its optical equivalent size; (2) the Impact Sensor (IS), a sensitive plate to measure the momentum released by each particles upon impact and (3) the Microbalances System (MBS), to measure the cumulative dust deposition from five different directions (Fig. 1). The GDS and the IS are placed in cascade along the path of the dust particle entering GIADA. In order to define and constrain the field of view of the instrument a short baffle is placed around the GIADA aperture (see Fig. 1). A dust particle entering GIADA first encounters the GDS, i.e. an illuminated area of 100 x 100 mm^2 with a thickness of 3 mm is generated by four pulsed (about 100 kHz) laser diodes emitting at $\lambda = 915$ nm; the scattered light produced by the crossing particle is detected by one of the two series (Right and Left receivers) of 4 centronic photodiodes equipped with a dedicated collimating optics and placed a 90° with respect to the laser propagation direction (y axis in Fig. 1). The signal is pre-elaborated by the proximity electronics in order to be amplified and to remove optical noise. The signal amplitude recorded by the receivers gives information on the optical equivalent size of the crossing particle while the time of flight across the curtain provides a first estimation of its speed (24). After crossing the

GDS the particle impacts the IS sensing plate: five zirconate piezoelectric (PZT) sensors glued underneath a 0.5 mm thick aluminum plate forming a 100 x 100 mm^2 sensitive area aligned to the GDS illuminated area. The five PZT sensors detect the acoustic bending wave generated by the impact and propagating across the plate. According to the mechanical properties of the aluminum plate, the PZTs have a flexural resonance frequency of 200 kHz and they convert the elastic deformation of the plate into an electrical signal. A peak and hold circuit in the proximity electronic of the sub-system register the amplitude of the signal that is linked to the momentum of the impacting particle. An additional PZT transducer glued under the plate produces a repeatable excitation signal, acting as an internal calibrator monitoring the IS responsivity during in-flight operations (25). The measurement of the time-of-flight between GDS and IS provides the speed of each individual particle entering GIADA. The mass of each impinging particle can be derived combining the momentum and speed measurements. The cumulative flux of particle with diameter $\leq$ 5 micron is measured by the MBS subsystem, a network of five Quartz Crystal Microbalances (QCM) pointing in different directions in order to characterize the dust flux within a view angle of 180° (Fig. 1). Each QCM consists of a matched pair of quartz crystals resonating at 15 MHz (26) having an acceptance angle of about 40° thanks to a small baffle mounted in front of the quartz sensors. The QCMs are equipped with a heating device to: (1) monitor the frequency vs. temperature dependence; (2) perform thermo-gravimetric measurements on the accumulated dust at temperatures up to 100 °C; and (3) measure the volatile vs. the refractory component (26).

3. Methods

The model philosophy adopted for GIADA foresaw the construction of two models of the instrument: a Proto Flight Model (PFM), now installed in a clean room in our laboratory, and a Flight Spare (FS) model, now onboard the Rosetta spacecraft. Both models were calibrated during the pre-launch campaign. During the Rosetta cruise and hibernation phases we decided to perform additional activities on pre-flight calibration data and to set-up an extended calibration campaign on the GDS and IS subsystems. This was decided for a two-fold reason: 1) an in depth re-analysis of the pre-flight calibration data highlighted specific weak points in the data reduction methods, e.g. a non accurate reconstruction of the particle impact position; 2) the

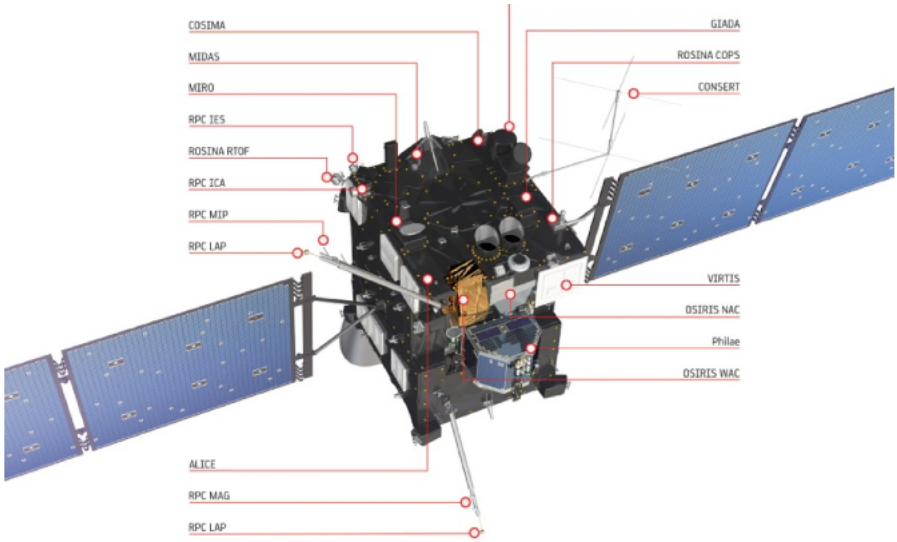

(a)

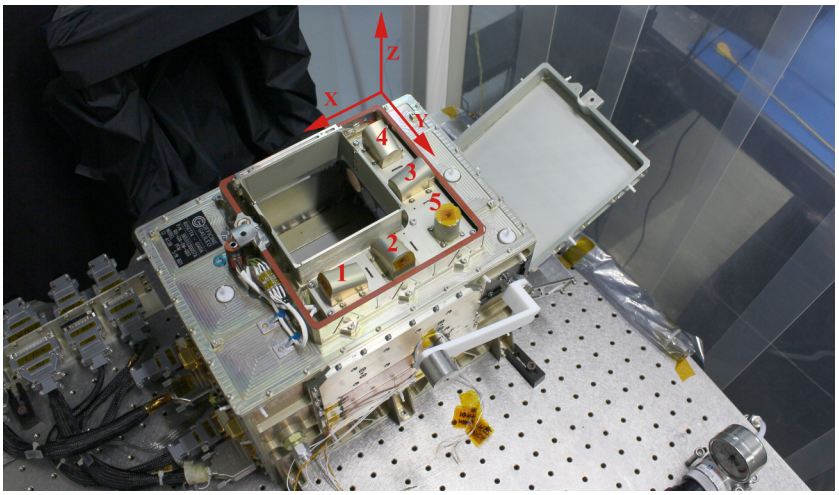

(b)

Figure 1: (a) Payload accommodated on the Rosetta spacecraft; GIADA is mounted on the nadir panel; (b) GIADA aperture where dust particles entering meet the GDS laser curtain and then impact on the IS at the bottom of the instrument; the five QCMs pointing in five different directions and forming the MBS are numbered in red.

increased knowledge on cometary dust, especially after the analyses of dust samples returned by the Stardust NASA mission from comet Wild2, encouraged us to derive a new set of response curves that would have optimized GIADA scientific results. For the extended calibration campaign we proceeded in three steps: 1) verify the IS responsivity and improve the method for particle impact position reconstruction; 2) analyse the GDS and IS physical response to a variety of cometary dust analogues in order to optimize the calibration curves; and 3) define transfer functions to correlate the two GIADA models, so to enable the use of the calibration curves obtained on GIADA PFM for GIADA FS.

3.1. IS responsivity and Impact position reconstruction

Given a constant momentum released by an impacting particle the signal of the five PZTs depends on the specific impact position on the aluminum plate. This effect is due to dissipative forces acting during wave propagation along the sensing plate. For a correct data analysis it is therefore pivotal to determine a sensitivity map for the sub-system (25) and a reliable algorithm for the impact position reconstruction. When a particle hits the IS plate in P^* (Fig 2) with coordinates (x_{imp}; y_{imp}), a flexural wave is produced and propagates along the plate as circular waves centered on the impact position. P^* coordinates can be reconstructed by means of the time counters connected to the PZTs that measure the time delays (starting from the first detection by one of the PZTs) with which the propagating wave reaches them. As soon as the wave front reaches the closest piezoelectric sensor, e.g. PZT 1 in the example sketched in figure 2, the time counters on the other PZTs are activated and then stopped when the propagating wave reaches them. Assuming a constant speed wave propagation, v=1.711 mm/μs (25), to reconstruct the impact position using the time delays with respect to PZT1, i.e. Δt2, Δt3, Δt4 and Δt5, an analytical solution can be applied. Due to the counters time resolution of 3μs the method can reconstruct the impact position within an error of 5x10^{-3}m (27). We first addressed the reliability of the analytical algorithm for the impact position reconstruction. For this analysis we used glass spheres, 500 μm in diameter, released by a rigid guide assuring a high precision on settled impact points. We performed ten launches on each point of a 9x9 grid, covering the whole IS sensitive surface. From equations:
P (x_{imp}, y_{imp})
$x_{imp} = A + r_0 * B$
$y_{imp} = C + r_0 * D$

$x_{imp}^2 + y_{imp}^2 = r_0^2 + E * r_0 + F.$
Where A, B, C, D, E and F are parameters depending on time delays, PZTs configuration and a, the aluminum plate side length, we reconstructed the impact positions and compared them with the settled impact points of the grid. To derive P^* coordinates, time delays from three out of five PZTs are sufficient. We used four different combinations of PZTs, reported as Comb (2,3,5), Comb (2,3,4), Comb (3,4,5) and Comb (2,4,5) in table 1, numbers refer to the corresponding PZTs. The results of the experiment to check the reliability of the impact position reconstruction are shown in table 1. The results are unsatisfactory, in fact most of the reconstructed positions differ from the actual impact positions for a distance greater than the uncertainty set by the IS hardware limits ($5\text{x}10^{-3}$m). *This difference is due to some residual cross talk among the amplification channel of each PZT. This behavior was highlighted between PZT2 and PZT1 signals. The error induced in the measurements of the time retard by this cross talk makes ineffective the theoretical algorithm for position reconstruction.* The ineffectiveness of the analytical method for the GIADA PFM, was a critical issue also for the GIADA FS onboard Rosetta. To overcome this issue we developed a new empirical method. The whole data set collected during GIADA development was analyzed and elaborated to obtain a look-up table linking impact positions to time delays. The table was obtained selecting the time delays recorded in correspondence of fixed impact positions over a 1 mm mesh grid covering the whole IS surface. The time delays (Δt1 to Δt5) measured during the experiments with glass spheres are compared with the values stored in the look-up table. The actual impact position is the one that in the look-up table has the same time delays. The results of this new method applied to the measurements performed during the extended calibration are reported in table 1, in columns labeled "New Method". This new method lead to the impact position reconstruction with a higher accuracy with respect to the old method. The old method is able to reconstruct the impact position, within the IS hardware limit only in 2 % of the trials, while with the new method the percentage rises to 20 %. Considering acceptable a maximum error of 20 mm, the new method provides results within this limit for the 60 % of the trials that compared to the 9 % obtainable with the old method represent a critical improvement. We reached even better results taking into account specific IS behaviors obtaining the impact position reconstruction, within 20 mm of accuracy, in 85 % of the trials. Such an accurate impact position reconstruction allowed us to rescale the IS signal by means of a sensitivity

map superseeding the issue of the non-uniformity sensing plate responsivity.

3.2. GDS+IS calibration to derive particle momentum and geometrical cross section

In order to calibrate the combined GDS+IS response we obtained GDS and IS calibration curves correlating the sub-systems response to the stimuli produced by well-characterized analog samples. We dropped or shot into GIADA PFM a statistically relevant number of particles (about 2000 in total) and we analyzed IS and GDS data versus particle momentum and optical cross-section as a function of composition, size and mechanical properties (Young Modulus) of the impacting particle. Cometary dust analogs were selected according to the recent knowledge gained through the analyses of interplanetary dust particles (28) and cometary samples returned from comet 81P/Wild2 (29; 3; 30). We prepared samples with sizes ranging from 20 μm to 500 μm in diameter following the hypothesized comet grain size distributions (31). The grains were produced in four distinct size bin: 1) $20 \leq \Phi \leq 50$ μm, 2) $50 \leq \Phi \leq 100 \mu$m, 3) $100 \leq \Phi \leq 250$ μm, and 4) $250 \leq \Phi \leq 500$ μm. The particles were characterized by multiple laboratory analytical techniques (32). Single particles were shot at velocities in the range of 0.8 to 100 ms^{-1} into the GIADA PFM using two different experimental setup. To obtain calibration curves linking GIADA measurements to particles physical and chemical properties we followed this procedure:

1. Using a camera connected to an optical stereo-microscope we acquired two images of each particle in two different positions (rotating the particle by 90°) deriving an average geometrical cross section (Fig. 5) and allowing the measurement of the three axes of the ellipsoid that best fits the particles. Once determined the three axes we calculated the volume of each particle from which we derived the mass, since the density of the selected materials was known.
2. We shot (or dropped) and measured into the GIADA PFM about 50 particles characterized in step 1, for each material. To shoot particles with sizes in the range 20-500 μm and speeds from 1 to 100 ms^{-1}, we used an air gun (Fig. 3a); for particle in the size range 250-500 μm with speeds ranging from 0.8 to 20 ms^{-1}, we used an electrostatic micro-manipulator (Fig. 3b) (33).
3. We measured the particle speeds from the time of flight between the GDS and IS detections (Fig. 4b) and combining them with the masses

Table 1: Verification of the reliability of the analytical method for the impact position reconstruction: comparison between the real impact positions settled a priori on the 9x9 grid mapping the IS plate and the reconstructed ones obtained by the analytical solution and by the new method. For the analytical solution we used 4 combination of PZTs for the reconstruction reported as Comb 2,3,5 Comb 2,3,4 Comb 3,4,5 and Comb 2,4,5, where the numbers are referred to the corresponding PZTs; in the last two columns on the right the coordinates obtained with the new developed method are reported

Real Impact Position		**Analytical Method** ($v = 1.711 mm/\mu s$)								**New Method**	
		Comb: 2, 3, 5		**Comb: 2, 3, 4**		**Comb: 3, 4, 5**		**Comb: 2, 4, 5**			
X[mm]	Y[mm]	X[mm]	Y[mm]	X[mm]	Y[mm]	X[mm]	Y[mm]	X[mm]	Y[mm]	X[mm]	Y[mm]
17	17	55.7	44.6	51.6	108.6	104.6	91.9	137.8	30.1	18.9	24.5
17	37	58.7	51.4	57.5	89.0	90.4	82.6	100.5	47.3	17.2	39.0
17	57	62.0	62.0	62.0	72.9	72.1	72.1	72.9	62.0	19.6	54.9
17	77	66.4	84.9	65.6	62.0	43.7	62.0	46.3	81.4	45.6	106.0
17	95	71.4	94.4	69.1	58.6	35.0	57.5	40.8	87.0	34.7	105.9
37	17	55.3	51.6	52.3	98.9	92.4	88.4	105.5	46.7	18.5	36.3
37	37	65.4	54.5	66.2	79.7	88.4	76.9	94.4	52.6	30.7	38.1
37	57	54.9	58.6	54.0	73.7	68.7	72.4	69.5	58.1	33.9	56.6
37	77	62.0	72.9	62.0	58.4	46.9	57.9	48.5	71.8	49.9	92.4
37	95	57.8	79.7	58.0	73.3	52.1	73.8	52.5	79.0	42.3	109.9
57	17	52.2	48.5	50.3	70.0	72.4	68.7	74.5	45.8	23.6	54.5
57	37	55.8	41.0	54.0	73.7	86.1	71.0	94.8	33.2	45.4	37.1
57	57	59.0	36.7	58.3	65.7	87.3	65.0	96.2	27.8	52.7	36.0
57	77	58.7	51.4	58.4	62.0	69.3	62.0	70.0	50.3	28.1	92.2
57	93	78.7	78.7	75.1	48.9	45.3	45.3	48.9	75.1	57.7	96.2
77	17	42.3	26.4	36.0	62.0	76.6	62.0	83.6	10.8	102.8	42.9
77	37	39.7	43.5	31.7	80.6	71.8	75.5	75.3	37.3	35.4	52.4
77	57	62.0	28.0	62.0	51.1	85.9	52.9	93.2	18.0	93.3	64.3
77	77	79.1	53.7	78.5	49.2	74.2	48.8	73.7	54.0	78.7	91.4
77	93	79.7	57.8	77.3	39.1	57.5	35.0	58.3	58.5	73.3	101.1
97	17	31.1	4.2	12.7	67.3	87.3	65.0	129.1	-89.4	105.3	29.5
97	37	40.3	19.9	32.1	62.0	80.3	62.0	92.3	-5.7	100.8	39.4
97	57	56.3	29.7	55.2	54.3	81.3	55.8	87.5	20.0	79.3	86.5
97	77	75.2	49.8	74.8	45.5	70.3	44.9	70.0	50.3	77	99.4
97	93	85.3	48.8	82.6	33.6	66.7	29.4	66.0	50.7	83.6	106.6

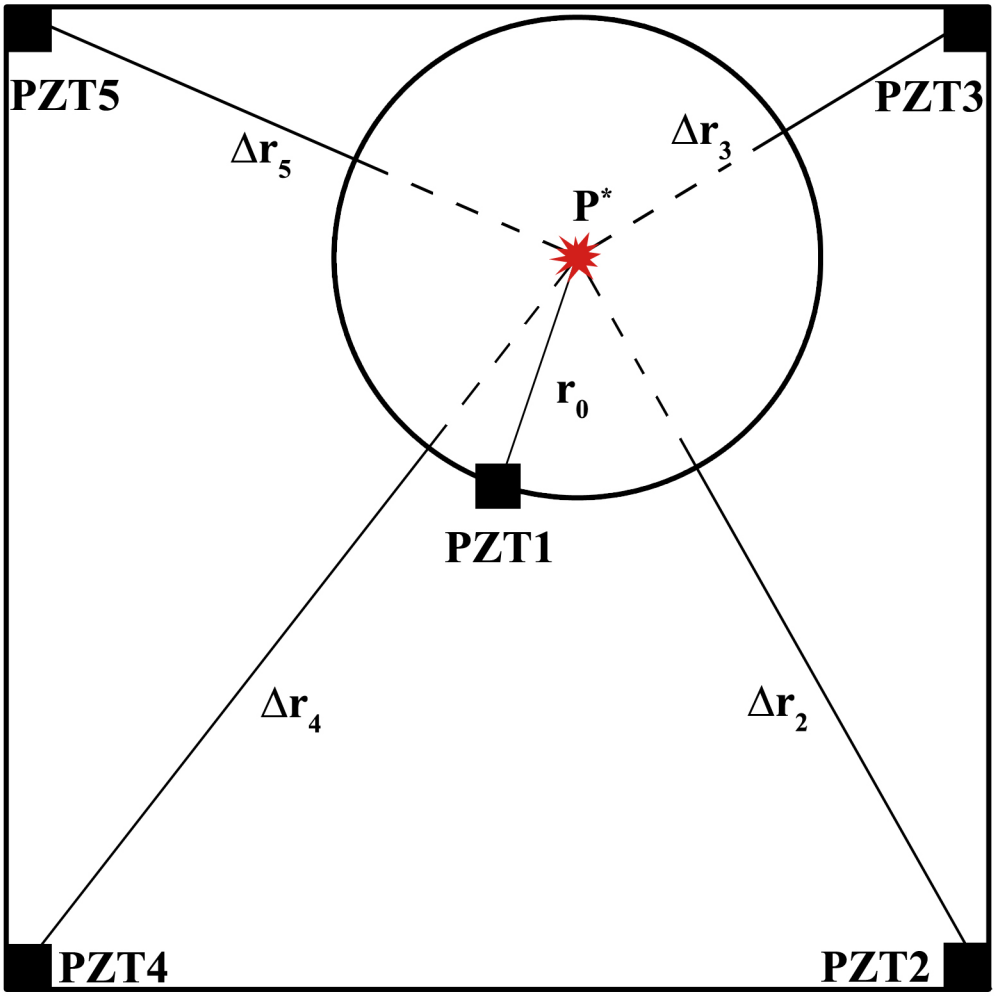

Figure 2: Reference frame and PZTs distribution used for the impact position reconstruction on the IS sensitive surface.

(a) **(b)**

Figure 3: Systems developed to shot particles: 3a) Air gun formed by a long small pipe connected to a small chamber where the particle is placed by means of a needle, the chamber is connected to a high pressure vessel through a valve actioned by a button; 3b) electrostatic device formed by 2 glass needle charged by a high voltage power supply.

derived at step 1, we calculated the actual particle momentum (Fig. 4c).

4. We recorded the GDS and IS signals, generated by the laser curtain crossing and by the impact on the sensing plate, of each particle.
5. The impact position for each impinging particle was reconstructed and the IS signal was rescaled according to the sensitivity map.

Following this procedure we obtained the calibration curves to link GIADA measurements to the physical and chemical properties of these particles.

4. Results

The extended calibration activities were mainly devoted to obtain the GIADA sub-system Response Function (RF) with respect to the particle momentum, speed and geometrical cross-section. To derive the IS-RF we proceeded in two steps: 1) analysis of the data collected shooting particles belonging to the whole set of cometary analogs selected to obtain an average IS-RF; 2) analysis of the data acquired for each type of cometary analog to obtain specific IS-RFs for each material. For the GDS, due to the high

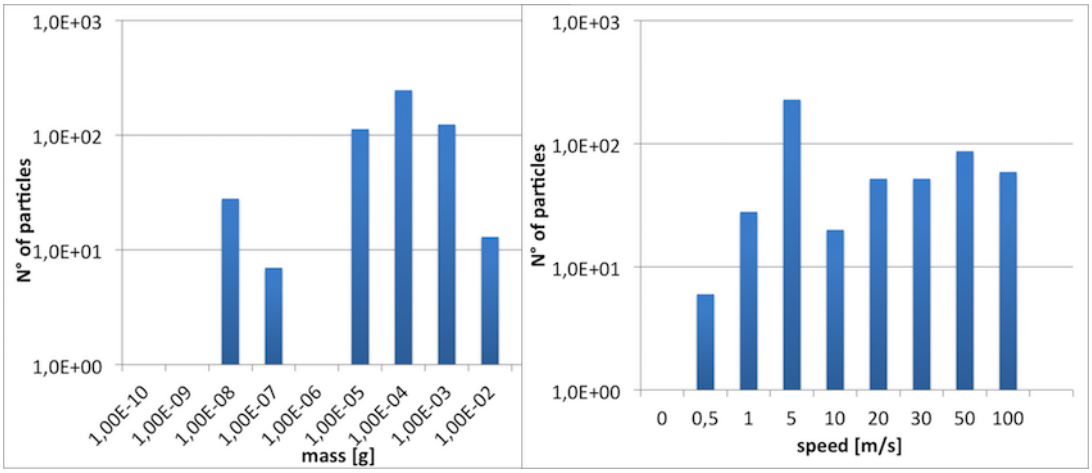

(a) **(b)**

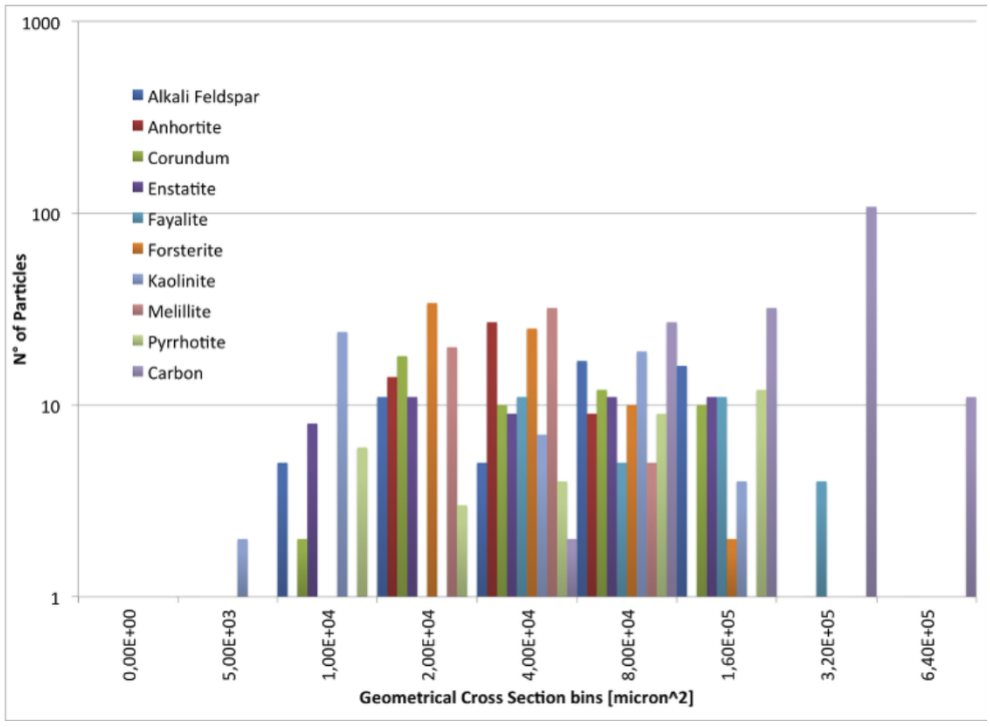

(c)

Figure 4: Momentum, speed and geometrical cross section of the particles used for the extended calibration campaign. 4a) Momentum distribution of the used particles; 4b) speed distribution of the used particles;4c) cross section distribution of the particles used for each analog material.

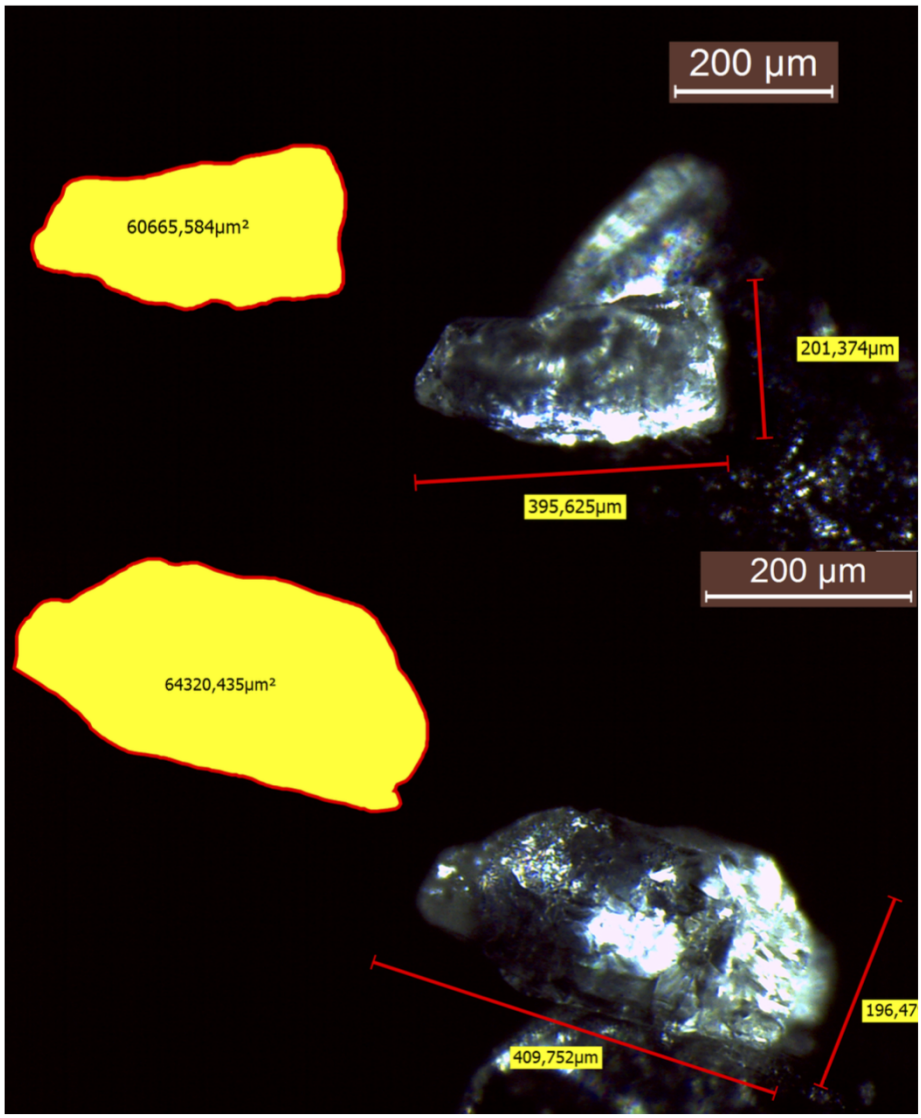

Figure 5: Two images of a forsterite grain belonging to the range 250-500μm taken with the Leica IC80HD camera attached to the Leica MC205 Microscope. The measured geometrical cross section and the axes measured in the two positions are reported. The needle used to manipulate the particles is visible on the background of the samples.

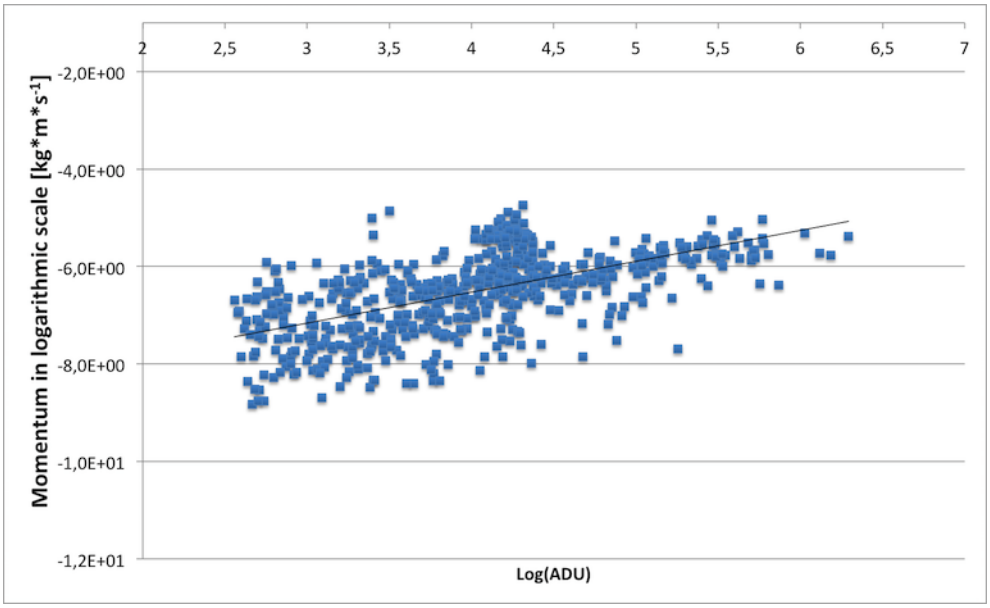

Figure 6: Correlation between momenta calculated with the procedure described in section 4.1 for each particle and the signal registered by the IS-PZT1 (GIADA PFM).

relevance on the GDS response of the optical property of the specific material, we derived only the GDS-RFs for each analog.

4.1. IS calibration curves

Thanks to the data obtained during the extended calibration phase we were able to obtain the average IS -RF. As an example, in Figure 6 we report the IS signals (digital units) acquired after launching a high number of particles ($\geq$ 200) belonging to the entire set of cometary analogs with respect to the actual particle momentum. In order to obtain the RF for each PZT a linear fit of the data (shown as an example in figure 6 for PZT1) was obtained and the parameters of the fits were calculated for all the five PZTs (table 2).

In order to investigate the IS response with respect to the impacting particle physical-chemical properties we analyzed the IS data for each analog material. This allowed us to evaluate the IS response with respect not only to the particle momentum but also to the kinetic energy. In fact, as all impacts conserve the momentum, what distinguishes different types of impacts is whether they also conserve kinetic energy. Collisions can either be

elastic, i.e. conserving both momentum and kinetic energy, or inelastic, i.e. conserving momentum but not kinetic energy. The degree to which a collision is elastic or inelastic is quantified by the restitution coefficient, ranging between zero (perfectly inelastic collision) and 1 (perfectly elastic collision). The interaction between the particle and the IS plate can be schematized in two stages. The first stage, purely elastic, starts at the initial contact between the particle and the plate and is characterized by the deformation of the particle. As the impact progresses, the pressure between the two bodies increases until the peak pressure reaches the particle elastic yield limit. The second stage, which lasts until the impacting bodies have a zero relative velocity, is characterized by the growth of a region of plastic deformation in the particle and in the impacted plate. It is assumed that the elastic yield limit remains constant throughout the impact. To understand if it is possible obtaining information on the tensile strength or the Young modulus of the impacting particles, we analyzed the IS readings with respect to both particle kinetic energy and momentum. This analysis, carried out for each selected material , allowed us to retrieve how the IS responsivity changes with respect to the elastic or inelastic impact type. In fact, the type of impact (elastic vs. inelastic) is linked to the Young modulus and to the elastic yield of the particle. Comparing the curve obtained fitting the momentum versus the IS signal for each material, we can retrieve the dependence of the IS calibration curve slope with respect to the particles Young modulus. Plotting the slope of the curve with respect to the particle Young modulus it can be seen that this slope increases for materials with higher Young modulus, i.e. with higher tensile strength (fig. 7). Thanks to this IS behavior, knowing the impact speed, an estimation of the particle tensile strength can be obtained. When the impact speed is not known, e.g. when the particle is not detected by the GDS, a rough estimation of the particle speed can be retrieved using the IS data. Analysing particle momentum vs. its kinetic energy, for a determined tensile strength, the ratio between these two quantities gives the particle speed.

4.2. GDS calibration curves

For the GDS subsystem the data analysis show a strong dependency of the particle geometrical cross section measurable with respect to the optical properties of the cometary analog crossing the GDS laser curtain (Fig. 8). Thus a function linking the GDS signal to the particle geometrical cross section has to take into account its composition. We grouped the geometrical

Table 2: IS Calibration curves obtained for the PFM: the parameters of each PZT are reported with the error on the parameter.

PZt	Slope	Intercept
PZt1	0.68 ±0.09	-9.18±0.35
PZt2	0.89 ±0.14	-9.62±0.48
PZt3	0.78 ±0.13	-9.33±0.48
PZt4	0.78 ±0.12	-9.05±0.41
PZt5	0.77 ±0.12	-9.19±0.44

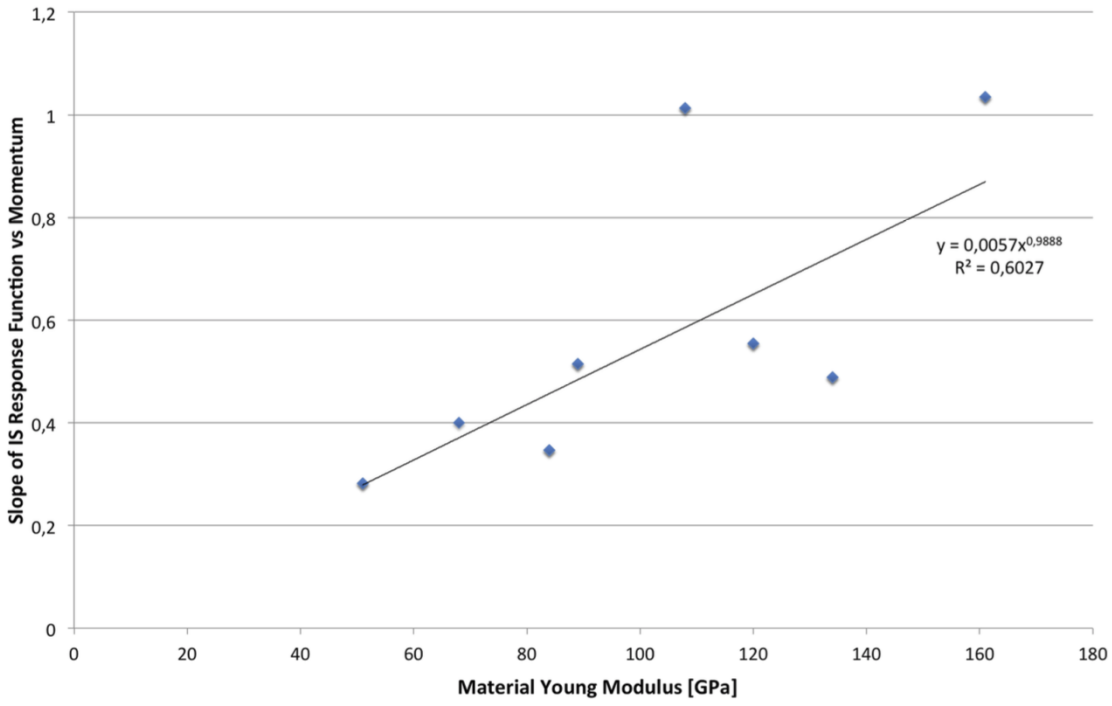

Figure 7: IS slopes of curves of IS RF obtained for each dust particle material w.r.t. the Young modulus of the material. An higher Young modulus correspond to an high IS responsivity.

cross-section values in different bins and evaluated their average and standard deviation. We computed the average and standard deviation for the corresponding bins of the GDS signal. We repeated this procedure for each type of cometary analog. We fitted the geometrical cross-section vs. GDS signal (for both Left and Right receivers). The algorithm of the regression to obtain the GDS fitting curve takes into account the average and the standard deviation of the points used for the fit, i.e. the average and the standard deviation evaluated for each cross-section and GDS signal bin. As examples we report in figure 9 the curves fitting the data, reported with their error bars, obtained by launching across the laser curtain alkali-feldspar, anorthite and melillite particles (Fig. 9a) and amorphous carbon particles (Fig. 9b). In figure 9a we merged data obtained for three different materials because their GDS response is very similar, i.e. the GDS is not able to differentiate their optical properties. For each cometary dust analog we are able to derive a calibration curve linking the particle geometrical cross-section with the GDS signal. The GDS curves are obtained using the following fitting model:
$CrossSection = A * Sign_{GDS}^{b}$
where A and b are the free parameters of the fit and $Sign_{GDS}$ is the signal obtained by the GDS. To obtain the fit parameter confidence intervals we applied the bootstrap method (34). Comparing the cometary analogs fit results, considering the confidence intervals obtained with the bootstrap method for the b parameter, all of the values are compatible with a single value: 2, i.e. about the mean value of the interval for all the materials. This behavior is true for both the receivers. The constant value 2 can be explained as an intrinsic characteristic of GDS data acquisition chain (detectors + proximity electronics). This result allowed us to separate the parameters affecting the GDS-RF. In fact, b is intrinsic of the acquisition chain while A can be assumed as a function of the average intensity of the laser curtain and of the particle scattering properties. We proceeded by fitting all the data with the equation
$CrossSection = A * Sign_{GDS}^{2}$
The obtained curves are plotted in Figure 10. The plots show that: 1) the geometrical cross section measurable by GDS depends on particle albedo; 2) materials with comparable optical properties have a similar GDS-RF; 3) both (Left and Right) receivers have the same trend with respect to the selected material.

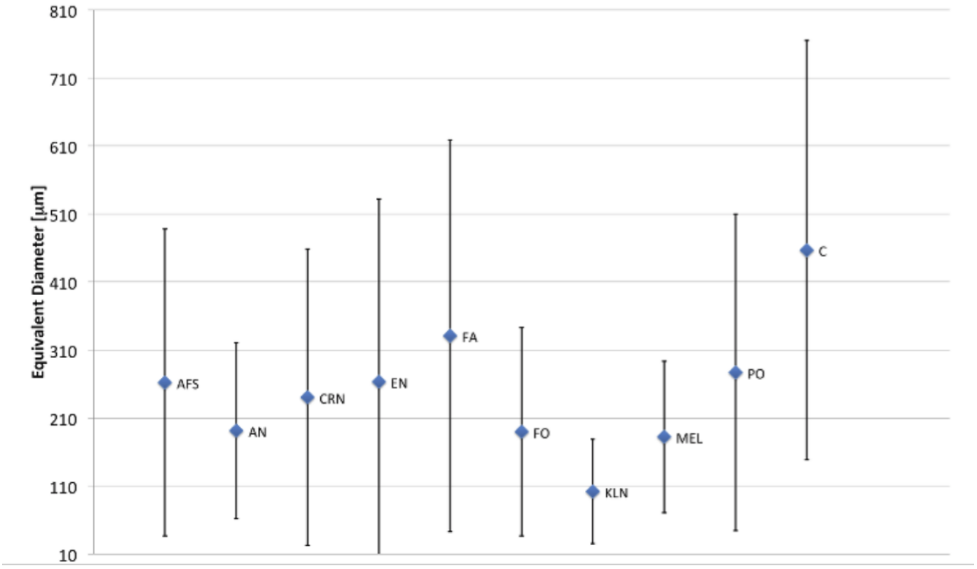

Figure 8: Size range of measurable particles by the GDS for each cometary analog.

4.3. Correlation between GIADA Proto Flight and Flight models

The calibration activity described above was performed using the GIADA PFM housed in a clean room in our laboratory. The results can be transferred to the GIADA FS, now operating onboard Rosetta. During pre-launch calibration campaign a major effort was made to characterize both GIADA models. In addition, during the Rosetta cruise phase and just before the comet escort phase, several tests on the GIADA FS were performed to check the sub-system status. Our work led us to reach the critical conclusion that IS and GDS calibration curves are linked to well defined, in both GIADA models, functional parameters, i.e. laser irradiance for the GDS and PZTs responsivity for the IS. In fact, these parameters can be derived for GIADA FS by means of the internal calibration devices: light monitors for laser irradiance, internal calibrator for PZTs responsivity. We could thus define simple IS and GDS transfer functions to rescale the GIADA PFM calibration curves to the GIADA FS.

5. Conclusions

The extended calibration campaign, performed during Rosetta cruise and hibernation phases on GIADA PFM, was planned to optimize GIADA FS sci-

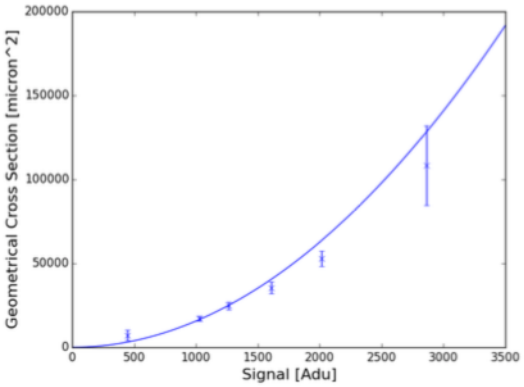

(a)

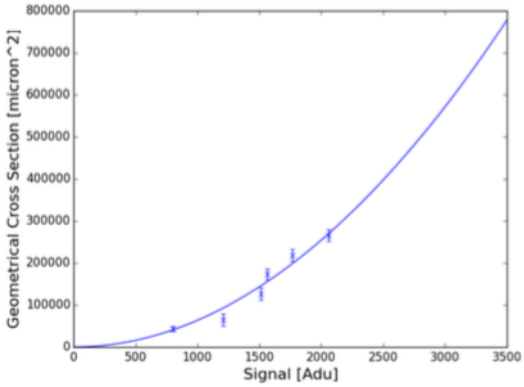

(b)

Figure 9: Measured particle geometrical cross sections versus GDS signal and their fitting curves: a) data obtained by launching across GDS alkali-feldspar, anorthite and melillite particles, which were group because of the GDS response similarity, i.e. GDS is unable to distinguish these three minerals having similar optical properties; b) data obtained by launching across GDS amorphous carbon particles.

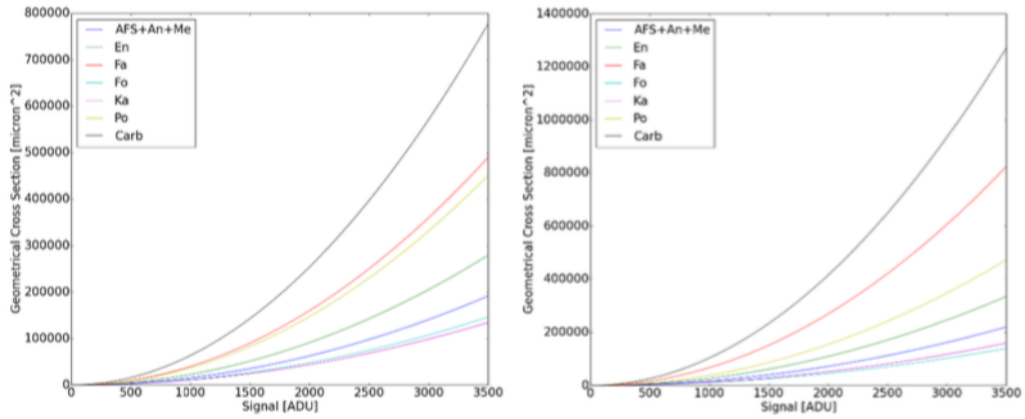

Figure 10: GDS IRF curves with respect to analog materials of particles: 10a) IRF of the right GDS channel; 10b) IRF of the left GDS channel.

entific data analyses. The review of the pre-launch calibration campaign data allowed us to recover a critical issue in the impact position reconstruction procedure. The newly developed method provides a reliable impact position reconstruction reducing considerably the error in the momentum measurements. To improve GIADA calibration exploiting the increased knowledge on cometary dust, we identified and produced a realistic set of cometary analogs referring to Wild2 dust particles laboratory analyses. For each analog we were able to determine calibration curves as a function of chemical-physical particle properties for the GIADA IS and GDS subsystems. The range of cometary analog types and the number of tests performed allowed us to investigate GIADA capability in constraining additional cometary dust particle physical properties. The IS response function dependence on the Young modulus of cometary dust analog was retrieved and will be used to constrain the tensile strength of 67P/C-G dust particles. We obtained a set of GDS calibration curves, which take into account particle composition. Thanks to these new curves we can derive particle geometrical cross sections that combined with measured masses allow us to derive dust particle density. Our work led us to define the correlation between GIADA PFM and GIADA FS. The complete datasets collected during the pre-launch calibration phase, performed on both models allowed us to obtain the transfer functions between the two GIADA models. This result permits the application of the new calibration curves to the GIADA FS data acquired on 67P/C-G dust.

6. Acknowledgements

GIADA was built by a consortium led by the Universit'a degli Studi di Napoli *Parthenope* and INAF - Osservatorio Astronomico di Capodimonte, in collaboration with the Instituto de Astrofisica de Andalucia, Selex-ES, FI, and SENER. GIADA is presently managed and operated by Istituto di Astrofisica e Planetologia Spaziali-INAF, Italy. GIADA was funded and managed by the Agenzia Spaziale Italiana, with the support of the Spanish Ministry of Education and Science Ministerio de Educacion y Ciencias (MEC). GIADA was developed from a Principal Investigator proposal from the University of Kent; science and technology contributions were provided by CISAS, Italy; Laboratoire d'Astrophysique Spatiale, France, and institutions from the UK, Italy, France, Germany, and the USA. Science support was provided by NASA through the U.S. Rosetta Project managed by the Jet Propulsion Laboratory/ California Institute of Technology. We would like to thank A. Coradini for her contribution as a GIADA Co-Investigator. GIADA calibrated data will be available through ESA's Planetary Science Archive (PSA) Web site (www.rssd.esa.int/index.php? project=PSApage=index). All data presented here are available on request before archival in the PSA. This research was supported by the Italian Space Agency (ASI) within the ASI-INAF agreements I/032/05/0 and I/024/12/0.

References

References

[1] F. J. Rietmeijer, Interplanetary dust particles, Planetary materials 36 (1998) 28–119.

[2] V. Della Corte, F. J. Rietmeijer, A. Rotundi, M. Ferrari, P. Palumbo, Meteoric cao and carbon smoke particles collected in the upper stratosphere from an unanticipated source, Tellus B 65.

[3] A. Rotundi, F. J. M. Rietmeijer, M. Ferrari, V. Della Corte, G. A. Baratta, R. Brunetto, E. Dartois, Z. Djouadi, S. Merouane, J. Borg, J. R. Brucato, L. Sergeant D'Hendecourt, V. Mennella, M. E. Palumbo, P. Palumbo, Two refractory Wild 2 terminal particles from a carrot-shaped track characterized combining MIR/FIR/Raman microspectroscopy and FE-SEM/EDS analyses, Meteoritics and Planetary Science 49 (2014) 550–575. doi:10.1111/maps.12274.

[4] S. A. Sandford, The collection and analysis of extraterrestrial dust particles, Fundamentals of Cosmic Physics 12 (1987) 1–73.

[5] V. Della Corte, P. Palumbo, A. Rotundi, S. De Angelis, F. J. Rietmeijer, E. Bussoletti, A. Ciucci, M. Ferrari, V. Galluzzi, E. Zona, In situ collection of refractory dust in the upper stratosphere: the duster facility, Space science reviews 169 (1-4) (2012) 159–180.

[6] D. Brownlee, P. Tsou, J. Aléon, C. M. O. . Alexander, T. Araki, S. Bajt, G. A. Baratta, R. Bastien, P. Bland, P. Bleuet, J. Borg, J. P. Bradley, A. Brearley, F. Brenker, S. Brennan, J. C. Bridges, N. D. Browning, J. R. Brucato, E. Bullock, M. J. Burchell, H. Busemann, A. Butterworth, M. Chaussidon, A. Cheuvront, M. Chi, M. J. Cintala, B. C. Clark, S. J. Clemett, G. Cody, L. Colangeli, G. Cooper, P. Cordier, C. Daghlian, Z. Dai, L. D'Hendecourt, Z. Djouadi, G. Dominguez, T. Duxbury, J. P. Dworkin, D. S. Ebel, T. E. Economou, S. Fakra, S. A. J. Fairey, S. Fallon, G. Ferrini, T. Ferroir, H. Fleckenstein, C. Floss, G. Flynn, I. A. Franchi, M. Fries, Z. Gainsforth, J.-P. Gallien, M. Genge, M. K. Gilles, P. Gillet, J. Gilmour, D. P. Glavin, M. Gounelle, M. M. Grady, G. A. Graham, P. G. Grant, S. F. Green, F. Grossemy, L. Grossman, J. N. Grossman, Y. Guan, K. Hagiya, R. Harvey, P. Heck, G. F. Herzog, P. Hoppe, F. Hörz, J. Huth, I. D. Hutcheon, K. Ignatyev, H. Ishii, M. Ito, D. Jacob, C. Jacobsen, S. Jacobsen, S. Jones, D. Joswiak, A. Jurewicz, A. T. Kearsley, L. P. Keller, H. Khodja, A. L. D. Kilcoyne, J. Kissel, A. Krot, F. Langenhorst, A. Lanzirotti, L. Le, L. A. Leshin, J. Leitner, L. Lemelle, H. Leroux, M.-C. Liu, K. Luening, I. Lyon, G. MacPherson, M. A. Marcus, K. Marhas, B. Marty, G. Matrajt, K. McKeegan, A. Meibom, V. Mennella, K. Messenger, S. Messenger, T. Mikouchi, S. Mostefaoui, T. Nakamura, T. Nakano, M. Newville, L. R. Nittler, I. Ohnishi, K. Ohsumi, K. Okudaira, D. A. Papanastassiou, R. Palma, M. E. Palumbo, R. O. Pepin, D. Perkins, M. Perronnet, P. Pianetta, W. Rao, F. J. M. Rietmeijer, F. Robert, D. Rost, A. Rotundi, R. Ryan, S. A. Sandford, C. S. Schwandt, T. H. See, D. Schlutter, J. Sheffield-Parker, A. Simionovici, S. Simon, I. Sitnitsky, C. J. Snead, M. K. Spencer, F. J. Stadermann, A. Steele, T. Stephan, R. Stroud, J. Susini, S. R. Sutton, Y. Suzuki, M. Taheri, S. Taylor, N. Teslich, K. Tomeoka, N. Tomioka, A. Toppani, J. M. Trigo-Rodríguez, D. Troadec, A. Tsuchiyama, A. J. Tuzzolino, T. Tyliszczak, K. Uesugi, M. Velbel, J. Vellenga, E. Vicenzi,

L. Vincze, J. Warren, I. Weber, M. Weisberg, A. J. Westphal, S. Wirick, D. Wooden, B. Wopenka, P. Wozniakiewicz, I. Wright, H. Yabuta, H. Yano, E. D. Young, R. N. Zare, T. Zega, K. Ziegler, L. Zimmerman, E. Zinner, M. Zolensky, Comet 81P/Wild 2 Under a Microscope, Science 314 (2006) 1711–. doi:10.1126/science.1135840.

[7] H. Yano, T. Kubota, H. Miyamoto, T. Okada, D. Scheeres, Y. Takagi, K. Yoshida, M. Abe, S. Abe, O. Barnouin-Jha, A. Fujiwara, S. Hasegawa, T. Hashimoto, M. Ishiguro, M. Kato, J. Kawaguchi, T. Mukai, J. Saito, S. Sasaki, M. Yoshikawa, Touchdown of the Hayabusa Spacecraft at the Muses Sea on Itokawa, Science 312 (2006) 1350–1353. doi:10.1126/science.1126164.

[8] A. Rotundi, H. Sierks, V. Della Corte, M. Fulle, P. J. Gutierrez, L. Lara, C. Barbieri, P. L. Lamy, R. Rodrigo, D. Koschny, et al., Dust measurements in the coma of comet 67p/churyumov-gerasimenko inbound to the sun, Science 347 (6220) (2015) aaa3905.

[9] M. Fulle, V. Della Corte, A. Rotundi, P. Weissman, A. Juhasz, K. Szego, R. Sordini, M. Ferrari, S. Ivanovski, F. Lucarelli, et al., Density and charge of pristine fluffy particles from comet 67p/churyumov–gerasimenko, The Astrophysical Journal Letters 802 (1) (2015) L12.

[10] Della Corte, V., Rotundi, A., Fulle, M., Gruen, E., Weissmann, P., Sordini, R., Ferrari, M., Ivanovski, S., Lucarelli, F., Accolla, M., Zakharov, V., Mazzotta Epifani, E., Lopez-Moreno, J. J., Rodriguez, J., Colangeli, L., Palumbo, P., al., et., Giada: shining a light on the monitoring of the comet dust production from the nucleus of 67p/churyumov gerasimenko, AAdoi:10.1051/0004-6361/201526208.
URL `http://dx.doi.org/10.1051/0004-6361/201526208`

[11] A. J. Tuzzolino, T. E. Economou, B. C. Clark, P. Tsou, D. E. Brownlee, S. F. Green, J. McDonnell, N. McBride, M. T. Colwell, Dust measurements in the coma of comet 81p/wild 2 by the dust flux monitor instrument, Science 304 (5678) (2004) 1776–1780.

[12] J. McDonnell, N. McBride, R. Beard, E. Bussoletti, L. Colangeli, P. Eberhardt, J. Firth, R. Grard, S. Green, J. Greenberg, et al., Dust particle impacts during the giotto encounter with comet grigg–skjellerup.

[13] J. C. Zarnecki, J. A. M. McDonnell, W. M. Burton, W. M. Alexander, M. S. Hanner, Mass distribution of particulates measured by Giotto's Dust Impact Detection System (DIDSY) in the close encounter period, in: B. Battrick, E. J. Rolfe, R. Reinhard (Eds.), ESLAB Symposium on the Exploration of Halley's Comet, Vol. 250 of ESA Special Publication, 1986, pp. 185–190.

[14] E. Gruen, H. Krueger, M. Landgraf, N. Altobelli, B. Anweiler, M. Baguhl, S. F. Dermott, V. Dikarev, N. Divine, H. Fechtig, A. L. Graps, B. A. Gustafson, D. P. Hamilton, M. S. Hanner, M. Horanyi, J. Kissel, B.-A. Lindblad, D. Linkert, G. Linkert, I. Mann, J. A. M. McDonnell, G. E. Morfill, C. Polanskey, R. Riemann, G. Schwehm, N. Siddique, R. Srama, P. Staubach, H. A. Zook, Ulysses Dust Detection System V3.1, NASA Planetary Data System 140.

[15] H.-J. Hoffmann, H. Fechtig, E. Gruen, J. Kissel, First results of the micrometeoroid experiment S 215 on the HEOS 2 satellite, 23 (1975) 215–224. doi:10.1016/0032-0633(75)90080-X.

[16] H. Dietzel, G. Eichhorn, H. Fechtig, E. Grun, H.-J. Hoffmann, J. Kissel, The HEOS 2 and HELIOS micrometeoroid experiments, Journal of Physics E Scientific Instruments 6 (1973) 209–217. doi:10.1088/0022-3735/6/3/008.

[17] D. H. Humes, J. M. Alvarez, W. H. Kinard, R. L. Oneal, Pioneer 11 meteoroid detection experiment - Preliminary results, Science 188 (1975) 473. doi:10.1126/science.188.4187.473.

[18] A. J. Tuzzolino, T. E. Economou, R. B. McKibben, J. A. Simpson, J. A. M. McDonnell, M. J. Burchell, B. A. M. Vaughan, P. Tsou, M. S. Hanner, B. C. Clark, D. E. Brownlee, Dust Flux Monitor Instrument for the Stardust mission to comet Wild 2, Journal of Geophysical Research (Planets) 108 (2003) 8115. doi:10.1029/2003JE002086.

[19] M. Horányi, Z. Sternovsky, M. Lankton, C. Dumont, S. Gagnard, D. Gathright, E. Grün, D. Hansen, D. James, S. Kempf, B. Lamprecht, R. Srama, J. R. Szalay, G. Wright, The Lunar Dust Experiment (LDEX) Onboard the Lunar Atmosphere and Dust Environment Explorer (LADEE) Mission, 185 (2014) 93–113. doi:10.1007/s11214-014-0118-7.

[20] G. Drolshagen, H. Svedhem, E. Grün, O. Grafodatsky, U. Prokopiev, Microparticles in the geostationary orbit (GORID experiment), Advances in Space Research 23 (1999) 123–133. doi:10.1016/S0273-1177(98)00239-7.

[21] A. Poppe, D. James, B. Jacobsmeyer, M. Horányi, First results from the Venetia Burney Student Dust Counter on the New Horizons mission, 37 (2010) 11101. doi:10.1029/2010GL043300.

[22] V. Della Corte, A. Rotundi, M. Accolla, R. Sordini, P. Palumbo, L. Colangeli, J. J. LopezMoreno, J. Rodriguez, F. J. M. Rietmeijer, M. Ferrari, F. Lucarelli, E. Mazzotta Epifani, S. Ivanovski, A. Aronica, M. Cosi, E. Bussoletti, J. F. Crifo, F. Esposito, M. Fulle, S. F. Green, E. Gruen, M. L. Herranz, J. M. Jeronimo, P. Lamy, A. Lopez Jimenez, J. A. M. McDonnell, V. Mennella, A. Molina, R. Morales, F. Moreno, E. Palomba, J. M. Perrin, R. Rodrigo, P. Weissman, V. Zakharov, J. C. Zarnecki, Giada: its Status after the Rosetta Cruise Phase and On-Ground Activity in Support of the Encounter with Comet 67P/CHURYUMOV-GERASIMENKO, Journal of Astronomical Instrumentation 3 (2014) 50011. doi:10.1142/S2251171713500116.

[23] L. Colangeli, J. J. Lopez Moreno, P. Palumbo, J. Rodriguez, E. Bussoletti, V. Della Corte, F. Esposito, M. Herranz, J. M. Jerónimo, A. Lopez-Jimenez, E. M. Epifani, R. Morales, E. Palomba, A. Rotundi, S. Vergara, International GIADA Team, GIADA: The Grain Impact Analyser and Dust Accumulator for the Rosetta space mission, Advances in Space Research 39 (2007) 446–450. doi:10.1016/j.asr.2006.12.048.

[24] E. M. Epifani, E. Bussoletti, L. Colangeli, P. Palumbo, A. Rotundi, S. Vergara, J. M. Perrin, J. J. L. Moreno, I. Olivares, The grain detection system for the GIADA instrument: design and expected performances, Advances in Space Research 29 (2002) 1165–1169. doi:10.1016/S0273-1177(02)00133-3.

[25] F. Esposito, L. Colangeli, V. Della Corte, P. Palumbo, Physical aspect of an "impact sensor" for the detection of cometary dust momentum onboard the "Rosetta" space mission, Advances in Space Research 29 (2002) 1159–1163. doi:10.1016/S0273-1177(02)00132-1.

[26] E. Palomba, E. L. Colangeli, P. Palumbo, A. Rotundi, J. M. Perrin, E. Bussoletti, Performance of micro-balances for dust flux measurement, Advances in Space Research 29 (2002) 1155–1158. doi:10.1016/S0273-1177(02)00131-X.

[27] A. Corallo, RO-GIA-IUNOAC-035TN, Tech. rep., Osservatorio Astronomico di Capodimonte (02 2000).

[28] F. J. M. Rietmeijer, Shower Meteoroids: Constraints From Interplanetary Dust Particles And Leonid Meteors, Earth Moon and Planets 88 (2002) 35–58. doi:10.1023/A:1013862627781.

[29] A. Rotundi, G. A. Baratta, J. Borg, J. R. Brucato, H. Busemann, L. Colangeli, L. D'Hendecourt, Z. Djouadi, G. Ferrini, I. A. Franchi, M. Fries, F. Grossemy, L. P. Keller, V. Mennella, K. Nakamura, L. R. Nittler, M. E. Palumbo, S. A. Sandford, A. Steele, B. Wopenka, Combined micro-Raman, micro-infrared, and field emission scanning electron microscope analyses of comet 81P/Wild 2 particles collected by Stardust, Meteoritics and Planetary Science 43 (2008) 367–397. doi:10.1111/j.1945-5100.2008.tb00628.x.

[30] F. J. M. Rietmeijer, Chemical identification of comet 81P/Wild 2 dust after interacting with molten silica aerogel, Meteoritics and Planetary Science 44 (2009) 1121–1132. doi:10.1111/j.1945-5100.2009.tb01212.x.

[31] F. J. M. Rietmeijer, J. A. Nuth, III, Grain sizes of ejected comet dust. Condensed Dust Analogs, Interplanetary Dust Particles and Meteors, in: L. Colangeli, E. Mazzotta Epifani, P. Palumbo (Eds.), The New Rosetta Targets. Observations, Simulations and Instrument Performances, Vol. 311 of Astrophysics and Space Science Library, 2004, p. 97.

[32] M. Ferrari, V. Della Corte, A. Rotundi, F. J. M. Rietmeijer, Single minerals, carbon- and ice-coated single minerals for calibration of GIADA onboard ROSETTA to comet 67P/Churyumov-Gerasimenko, 101 (2014) 53–64. doi:10.1016/j.pss.2014.06.006.

[33] R. Sordini, M. Accolla, V. Della Corte, A. Rotundi, GIADA: extended calibration activity: . the Electrostatic Micromanipulator, Memorie della Societa Astronomica Italiana Supplementi 26 (2014) 128.

[34] B. Efron, R. J. Tibshirani, An introduction to the bootstrap, CRC press, 1994.